Available online at www.sciencedirect.com
SCIENCE DIRECT®
Polyhedron 24 (2005) 189–200
POLYHEDRON
www.elsevier.com/locate/poly

Syntheses, photoluminescence and electroluminescence of some new blue-emitting phosphorescent iridium(III)-based materials

Inamur R. Laskar, Shih-Feng Hsu, Teng-Ming Chen *

Department of Applied Chemistry, National Chiao Tung University, Hsinchu 30055, Taiwan

Received 20 August 2004; accepted 29 October 2004
Available online 22 December 2004

Abstract

The cyclometallated ligand 2-(4′,6-difluorophenyl)-4-methoxypyridine (F_2MeOppyH), whose complexes with iridium(III) emit bright blue to green light, was synthesized in five separate steps. Ir(F_2MeOppy)$_2$(acac), (acacH = 2,4-pentanedione), Ir(F_2MeOppy)$_2$(pic) (picH = 2-picolinic acid), *fac*-Ir(F_2MeOppy)$_3$ and *mer*-Ir(F_2MeOppy)$_3$ complexes were synthesized from solution and fully characterized. The structures of Ir(F_2MeOppy)$_2$(acac) and *fac*-Ir(F_2MeOppy)$_3$ were authenticated by X-ray single crystal structure analysis. *fac*-Ir(F_2MeOppy)$_3$ showed a much higher solution photoluminescence (PL) quantum efficiency and blue-shifted emission compared to its counter *mer*-isomer. All of the complexes showed reversible oxidations between 0.3 and 0.7 V versus the ferrocene/ferrocenium ion. The relative thermodynamic stability of the *mer* versus *fac* isomer was investigated and correlated to their corresponding redox and PL properties. Two electroluminescent (EL) devices (D-1 and D-2) were fabricated using the same blue Ir(F_2MeOppy)$_2$(acac) complex as a a dopant but with two different hole blockers, BCP and BAlq, and consequently BCP proved itself a good hole blocker for this type of system. The fabrication of another EL device (D-3) was carried out by using the same dopant, only replacing the host CBP by a wider band gap host, *m*CP which showed improved luminance, luminance yield and power efficiency (D-2: 133 cd m^{-2}, 0.66 cd A^{-1}, 0.22 lm W^{-1}; D-3: 326 cd m^{-2}; 1.63 cd A^{-1}; 0.26 lm W^{-1}).

Keywords: Facial; Meridional; Iridium(III) complex; Blue phosphorescent; Photoluminescence; Electroluminescence

1. Introduction

Syntheses of materials based on heavy metal (Ir(III), Pt(II), Os(II), Re(I)) complexes, used as phosphorescent dopants, have attracted a great deal of attention due to their potential applications in organic light emitting devices (OLEDs) [1–4]. Of the above heavy metal-containing phosphor emitters that have been reported in OLEDs, cyclometallated complexes of iridium(III) materials have shown the most promising applications due to their higher stability, higher photoluminescence (PL) efficiency and relatively shorter excited state lifetime. Purely green- and red-emitting phosphorescent complexes of iridium(III) [5] are common, whereas the purely blue-emitting complex dopants [6] are scarcely found. Hence, the current effort of scientists has been focused on the syntheses of blue-emitting iridium(III)-based materials.

Amongst the complexes, the syntheses of Ir(F_2ppy)$_2$(acac) and Ir(F_2ppy)$_2$(pic) (F_2ppy = 2-(2′, 4′-difluorophenyl)pyridine; acacH = 2,4-pentanedione; picH = 2-picolinic acid) [7] are notable examples for blue-emitting materials. Recently, Coppo et al. [8] reported the blue-emitting phenylpyridine iridium(III) complexes using triazolyl pyridine types as ancillary ligands. In this work, we have introduced strong electron donating substituents at the 4-position of the LUMO containing pyridyl moiety in 2-(2′,4′-difluorophenyl)pyridine, which is

* Corresponding author. Tel.: +8865712121x56526; fax: +88635723764.
E-mail address: tmchen@mail.nctu.edu.tw (T.-M. Chen).

0277-5387/$ - see front matter © 2004 Elsevier Ltd. All rights reserved.
doi:10.1016/j.poly.2004.10.016

supposed to further raise the LUMO energy state of the corresponding iridium(III) complex. Hence, the energy gap will be enhanced and consequently result in a more hypsochromic shift when compared to the parent complex. Our first choice was to incorporate a methoxy substituent at the 4-position of the pyridyl moiety in 2-(2,4′-difluorophenyl)pyridine. We have also synthesized both the *fac*-/*mer*-isomers of the same ligand, investigated and differentiated their photoluminescence and redox behaviors as well as their thermal stability. We report on the syntheses of four blue-emitting iridium(III) complex dopants using the same cyclometallated ligand, 2-(2′,4′-difluorophenyl)-4-methoxypyridine, and characterization and detailed studies of their photophysical as well as redox properties, X-ray single-crystal structure analyses of $Ir(F_2MeOppy)_2(acac)$ and *fac*-$Ir(F_2MeOppy)_3$ and the application of $Ir(F_2MeOppy)_2(acac)$ as a dopant in electroluminescent (EL) devices.

2. Experimental

2.1. Materials

$IrCl_3 \cdot 3H_2O$ was purchased from Alfa Aesar, USA, 2,4-difluoroboronic acid, picolinic acid and glycerol from Aldrich Chemicals, USA and the remaining compounds from Tokyo Kasei Kogyo Co. Ltd., Japan, and all were used as received.

2.2. Syntheses

2-Chloropyridine-N-oxide (yield 95%): 2-Chloropyridine was allowed to react with excess *m*-chloroperoxybenzoic acid in dichloromethane at ~0 °C, for 16 h. Then, the volume of the solvent was reduced to half and it was passed through a basic alumina bed using dichloromethane as an eluent, which resulted in pure 2-chloropyridine-N-oxide. ^1H NMR (300 MHz, $CDCl_3$): δ 8.39 (t, 1H, *J* 3.9 Hz), 7.54 (t, 1H, *J* 5.1 Hz), 7.27 (m, 2H). EIMS: *m*/*z* 130, Calc. 130.5.

2-Chloro-4-nitropyridine-N-oxide (yield 70%) [9]: 2-chloropyridine-N-oxide (10 g) was added to conc. sulfuric acid (15 ml) at 0–5 °C. Then, a mixture of conc. sulfuric acid (15 ml) and fuming nitric acid (30 ml) (sp. gr. 1.5) was added dropwise with stirring at 1–2 °C over a 45-min period. The mixture was heated slowly to 90 °C over 1 h and then maintained at 90 °C with stirring for an additional hour after which the mixture was cooled to 10 °C, poured into a stirred ice–water mixture, and neutralized with sodium carbonate. The yellow precipitate was collected, air-dried, and then recrystallized from an ethanol–chloroform mixture. ^1H NMR (300 MHz, $CDCl_3$): δ 8.45 (m, 2H), 8.04 (m, 1H). EIMS: *m*/*z* 176, Calc. 175.5.

2-Chloro-4-nitropyridine (yield 90%) [9]: 2 g of 2-chloro-4-nitropyridine-N-oxide was taken in 30 ml of ethyl acetate and ~3 ml of phosphorous tribromide was added slowly. Then, the mixture was heated with stirring at 70 °C for 10 min. The mixture was cooled, poured into an ice–water mixture, made alkaline to litmus with 10% aqueous sodium hydroxide and extracted with chloroform. The solvent was evaporated and purified by column chromatography. ^1H NMR (300 MHz, $CDCl_3$): δ 8.67 (dd, 1H, *J* 0.5, 5.4 Hz), 8.20 (d, 1H, *J* 1.8 Hz), 7.99 (dd, 1H *J* 1.8, 5.4 Hz). EIMS: *m*/*z* 158, Calc. 158.5.

2-Chloro-4-methoxypyridine (yield 55%): 2-Chloro-4-nitropyridine (1 eq.) was reacted with sodium methoxide (1.3 eq.) in dioxane at 100 °C for 12 h. The reaction mixture was cooled to room temperature and poured into water. Then, the organic layer was separated out and the aqueous layer was washed by ethyl acetate. The combined organic extracts were dried and evaporated to dryness. The compound was purified by column chromatography. ^1H NMR (300 MHz, $CDCl_3$): δ 8.43 (d, 1H, *J* 6 Hz), 7.26 (d, 1H, *J* 2.1 Hz), 7.06 (m, 1H). EIMS: *m*/*z* 143, Calc. 143.5.

2-(2′,4′-Difluorophenyl)-4-methoxypyridine (yield 80%) [10]. 5 g of 2-chloro-4-methoxy pyridine (1 eq.), 8.8 g of 2,4-difluorophenylboronic acid (1.6 eq.) and 1.15 g of triphenylphosphine (0.1 eq.) were dissolved in 1,2-dimethoxyethane (50 ml). 60 ml of 2 M K_2CO_3 (2.7 eq.) aqueous solution was added and the mixture was purged with argon gas. 0.25 g of palladium acetate (0.025 eq.) was added and the mixture was refluxed for 18 h. The two phases were then separated and the aqueous phase was extracted with ethyl acetate. The combined organic phases were washed with water and brine, successively, and then dried over $MgSO_4$. After evaporation of the solvent, the pure product was obtained by column chromatography. ^1H NMR (300 MHz, $CDCl_3$): δ 8.51 (d, 1H, *J* 5.7 Hz), 7.98 (m, 1H), 7.26 (t, 1H, *J* 2.1 Hz), 6.94 (m, 2H), 6.78 (dd, 1H, *J* 2.4, 5.7 Hz), 3.87 (s, 3H). EIMS: *m*/*z* 221, Calc. 221.

$(F_2MeOppy)_2Ir(\mu\text{-}Cl)Ir(F_2MeOppy)_2$ (yield 75%) [5e–5f]. Calc. for $C_{48}H_{32}N_4O_4F_8Cl_2Ir_2$: C, 43.1; H, 2.4; N, 4.2. Found: C, 43.0; H 2.3; N 4.0%. A solution of $IrCl_3 \cdot 3H_2O$ (1 mmol) and 2-(2′,4′-difluorophenyl)-4-methoxypyridine (3 mmol) in 2-ethoxyethanol (30 ml) was refluxed for 24 h. The pale green mixture was cooled to room temperature and 20 ml of 1 M HCl was added to precipitate the product. The mixture was filtered and washed with 100 ml of 1 M HCl followed by 50 ml of methanol, and then dried. The product was obtained as a light green powder. ^1H NMR (300 MHz, $CDCl_3$): δ 8.91 (d, 4H, *J* 6.6 Hz), 7.80 (s, 4H), 6.43 (m, 4H), 6.31 (t, 4H, *J* 9.9 Hz), 5.37 (d, 4H, *J* 9.0 Hz), 4.01 (s, 12H). FABMS: *m*/*z* 1335, Calc. 1335.

$Ir(F_2MeOppy)_2(acac)$ (yield 85%) [5e–5f]. Calc. for $C_{29}H_{23}N_2O_4F_4Ir$: C, 47.6; H, 3.1; N, 3.8. Found: C, 47.3; H 3.1; N 3.6%. $(F_2MeOppy)_2Ir(\mu\text{-}Cl)Ir(F_2MeOp-$

$py)_2$ (1 mmol), acetylacetone (3 mmol) and sodium carbonate (10 mmol) were mixed in 10 ml of 2-ethoxyethanol. The mixture was refluxed under nitrogen for 12 h. The reaction mixture was then cooled and the pale green precipitate was filtered off. The product was washed by methanol several times, followed by hexane. Then it was recrystallised from the mixture of dichloromethane and methanol (1:1). ^{1}H NMR (300 MHz, $CDCl_3$): δ 8.19 (d, 2H, *J* 6.6 Hz), 7.75 (s, 2H), 6.76 (dd, 2H, *J* 2.5, 6.3 Hz), 6.30 (t, 2H, *J* 10.5 Hz), 5.70 (d, 2H, *J* 7.2 Hz), 5.22 (s, 1H), 4.20 (s, 6H), 1.85 (s, 6H). FABMS: *m*/*z* 731, Calc. 731.

$Ir(F_2MeOppy)_2$(pic) (yield 92%) [6d]. Calc. for $C_{30}H_{20}N_3O_4F_4Ir_2$: C, 47.7; H, 2.7; N, 4.8. Found: C, 47.6; H 2.6; N 4.8%. 2.2 mmol of picolinic acid was added to a room temperature solution of 0.8 mmol of $(F_2MeOppy)_2Ir(\mu\text{-}Cl)Ir(F_2MeOppy)_2$ in 60 ml of dichloromethane. The mixture was heated to reflux under nitrogen in an oil bath for 16 h. The reaction mixture was cooled to room temperature and the pale yellow precipitate was filtered off. The pure product was obtained by flash chromatography. ^{1}H NMR (300 MHz, $CDCl_3$): δ 8.48 (d, 1H, *J* 6.9 Hz), 8.32 (d, 1H, *J* 7.2 Hz), 7.92 (t, 1H, *J* 6.6 Hz), 7.76 (m, 3H), 7.40 (td, 1H, *J* 1.5, 5.7 Hz), 7.17 (d, 1H, *J* 6.6 Hz), 6.73 (dd, 1H, *J* 2.7, 6.9 Hz), 6.53 (dd, 1H, *J* 2.7, 6.6 Hz), 6.42 (m, 2H), 5.88 (dd, 1H, *J* 2.3, 8.7 Hz), 5.64 (dd, 1H, *J* 2.6, 8.7 Hz), 4.06 (s, 6H). FABMS: *m*/*z* 754, Calc. 754.

mer-$Ir(F_2MeOppy)_3$ (yield 60%) [6a]. Calc. for $C_{36}H_{24}N_3O_3F_6Ir$: C, 50.7; H, 2.8; N, 4.2. Found: C, 50.5; H 2.7; N 4.0%. 1 equivalent of $(F_2MeOppy)_2Ir(\mu\text{-}Cl)$ $Ir(F_2MeOppy)_2$, 2 equivalents of the cyclometallated ligand ($F_2MeOppyH$) and 10 equivalents of sodium carbonate were mixed and refluxed in 2-ethoxyethanol for 20 h. The reaction was then allowed to cool to room temperature and distilled water was poured down on it. Immediately, the impure product was precipitated out and it was purified by flash chromatography by using dichloromethane as an eluant. ^{1}H NMR (300 MHz, $CDCl_3$): δ 7.77 (m, 3H), 7.64 (m, 2H), 7.31 (t, 1H, *J* 7.5 Hz), 6.64 (td, 1H, *J* 2.1, 7.9 Hz), 6.52 (td, 2H, *J* 3.0, 6.6 Hz), 6.39 (m, 4H), 6.06 (dd, 1H, *J* 2.4, 7.5 Hz), 5.88 (dd, 1H, *J* 2.4, 9.3 Hz), 4.14 (s, 9H). FABMS: *m*/*z* 852, Calc. 852.

fac-$Ir(F_2MeOppy)_3$ (yield 50%) [6a]. Calc. for $C_{36}H_{24}N_3O_3F_6Ir$: C, 50.7; H, 2.8; N, 4.2. Found: C, 50.4; H 2.7; N 4.1%. 1 equivalent of $Ir(F_2MeOppy)_2$(acac) and 1.5 equivalents of the cyclometallated ligand ($F_2MeOppyH$) were refluxed in glycerol for 24 h. Then the reaction mixture was cooled to room temperature and distilled water was added to it. The impure product was separated out and purified by flash chromatography. ^{1}H NMR (300 MHz, $CDCl_3$): δ 7.39 (s, 3H), 7.28 (d, 3H, *J* 6.6 Hz), 6.50 (t, 3H, *J* 4.2 Hz), 6.31 (m, 2H), 4.11 (s, 9H). FABMS: *m*/*z* 852, Calc. 852.

2.3. Crystallography

Single crystal diffraction data for $Ir(F_2MeOppy)_2$(acac) and *fac*-$Ir(F_2MeOppy)_3$ were collected on a Bruker Smart CCD diffractometer equipped with a normal focus, 3kW sealed-tube X-ray source (λ = 0.71073 Å). The intensity data were collected in the ω scan mode (width of 0.3/° frame) and corrected for *Lp* and absorption effects by using the SAINT [11] program. Cell refinement and data reduction were carried out by using the program Bruker SHELXTL [12] and the crystal structure was solved by direct methods using the SHELXTL [12] version 5.1 software packages. The structure was further refined by full-matrix least-squares methods based on F^2 using SHELXTL version 5.1 [12]. Positions of non-hydrogen atoms were refined anisotropically, whereas the hydrogen positions were not refined.

2.4. Optical measurements and compositions analysis

The ultraviolet-visible (UV–Vis) spectra of the phosphorescent Ir(III) complexes were measured on an UV–Vis spectrophotometer (Agilent model 8453) and corrected for background due to solvent absorption. Photoluminescence (PL) spectra were carried out with a spectrophotometer (Jobin-Yvon Spex, model Fluorolog-3). Emission quantum yields were measured by the method of Demas and Crosby [13] using *fac*-$Ir(ppy)_3$ as a reference [14]. NMR spectra were recorded on Varian 300 MHz. MS spectra (EI and FAB) were taken by micromass TRIO-2000. Cyclic voltammetry (CV) analyses were performed by using CHI 2.05; dichloromethane was used as a solvent in an inert atmosphere and 0.1 M tetra(*n*-butyl)ammonium tetrafluoroborate was used as the supporting electrolyte. A glassy carbon rod was used as the working electrode, platinum was used as the counter electrode and a silver wire was used as a pseudo-reference electrode. The TG-DTA analysis was carried out by using a thermal analyzer (SEIKO 1TG/DTA model 200). Emission lifetimes were obtained by exponentially fitting the emission decay curves recorded on Continuum model NY61 spectrofluorometer.

2.5. OLED fabrication and testing

In the fabrication of OLEDs organic layers were thermally evaporated onto a glass substrate precoated with an indium–tin–oxide (ITO) layer with a sheet resistance of 20 Ω under high-vacuum. Prior to use, the ITO surface was ultrasonicated in a detergent solution followed by rinsing with deionized (DI) water, dipped into acetone, trichloroethylene and 2-propanol, and then degreased with a vapor of 2-propanol. After degreasing, the substrate was oxidized and cleaned in a UV-ozone chamber before it was loaded into an evaporator. In a vacuum chamber at a pressure of 10^{-6} Torr, 500 Å of

NPB as the hole transporting layer; 200 Å of the complex doped (7%) CBP as the emitting layer; 100 Å of 2,9-dimethyl-4,7-diphenyl-1,10-phenanthroline (BCP) as a hole and exciton blocking layer (HBL); 650 Å of Alq_3 as the electron transport layer; and a cathode composed of 10 Å lithium fluoride and 2000 Å aluminum were sequentially deposited onto the substrate to give the device structure. The current–voltage (*I–V*) profiles and light intensity characteristics for the above-fabricated devices were measured in a vacuum chamber of 10^{-6} Torr at ambient temperature using a Keithley 2400 Source Meter/2000 Multimeter coupled to a PR 650 Optical Meter.

3. Results and discussion

3.1. Synthesis

The ligand, 2-(2′,4′-difluorophenyl)-4-methoxypyridine (F_2MeOppyH) has been synthesized in five separate steps smoothly (Scheme 1; see experimental part). The yield of 4-methoxy-2-chloro-pyridine (4th step) is relatively poor (~55%) as compared to the other intermediates and the final compound (F_2MeOppyH). $IrCl_3 \cdot 3H_2O$ was allowed to react with an excess of F_2MeOppyH to give chloride-bridged dinuclear complex [5e,5f]. The mononuclear complexes, Ir(F_2MeOppy)$_2$(acac) and Ir(F_2MeOppy)$_2$(pic) have been synthesized [5e,5f] by replacing the bridging chlorides from the dinuclear species (Scheme 2), with bidentate, monoanionic acetylacetonate and picolinate, respectively. The proton NMR spectra of these complexes are consistent with the heterocyclic rings of the cyclometallated ligand being in a *trans*-disposition. The tris-isomeric complexes (*facial/meridional*) have also been synthesized by varying the temperature and using the cyclometallated ligand, F_2MeOppyH. Thompson et al. [6a] reported the syntheses of the *mer*-isomer at 140 °C and the *fac*-isomer of iridium(III) complexes at 200 °C along with little amount of *mer*-isomer as a by-product. In our case, the *meridional* form has been synthesized at a relatively lower temperature (~120 °C), whereas the synthesis at higher temperature (~200 °C) generates absolutely the *facial* form (Scheme 2). We have always isolated a mixture of *fac* and *mer* isomers at 140 °C. Furthermore, pure *mer*-isomer was taken in glycerol and refluxed for 24 h. It was observed that the *mer*-isomer converted to the *fac*-isomer almost completely, inferring that the *mer*-isomer was a kinetically controlled product, whereas the *fac*-isomer was favored thermodynamically. These isomers could also been differentiated clearly on the TLC plate due to their large polarity differences. ^{1}H NMR and ^{19}F NMR spectra (Fig. 1) clearly distinguished the *fac*-isomer from the *mer*-form. In ^{19}F spectra, we observed two peaks for the inherent-C_3 symmetric *facial* isomer and the six peaks for the asymmetric *mer*-isomer. Furthermore, TGA-DTA studies showed that the complexes are stable up to 340–360 °C and they can be sublimed easily under a pressure of 10^{-3} mm Hg.

3.2. X-ray crystallography

Single crystals of Ir(F_2MeOppy)$_2$(acac) and *fac*-Ir(F_2MeOppy)$_3$ were grown from methanol/dichloromethane (1:1) and chloroform, respectively, and characterized using X-ray crystallography. The ORTEP drawings of Ir(F_2MeOppy)$_2$(acac) and *fac*-Ir(F_2MeOppy)$_3$ are represented in Figs. 2(a) and (b), respectively. The crystal data and the selected bond lengths of both complexes are displayed in Tables 1 and 2, respectively. The dispo-

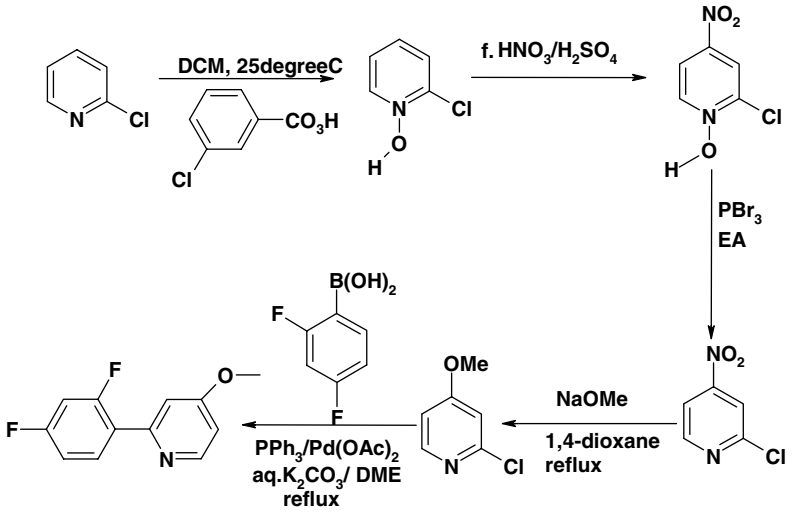

Scheme 1.

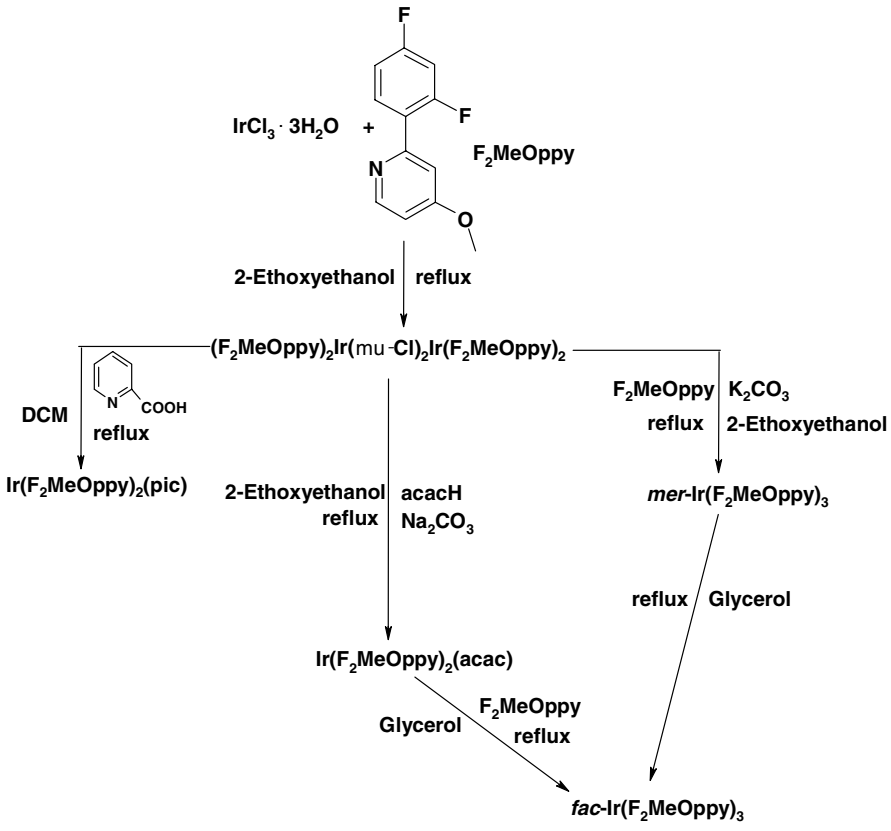

Scheme 2.

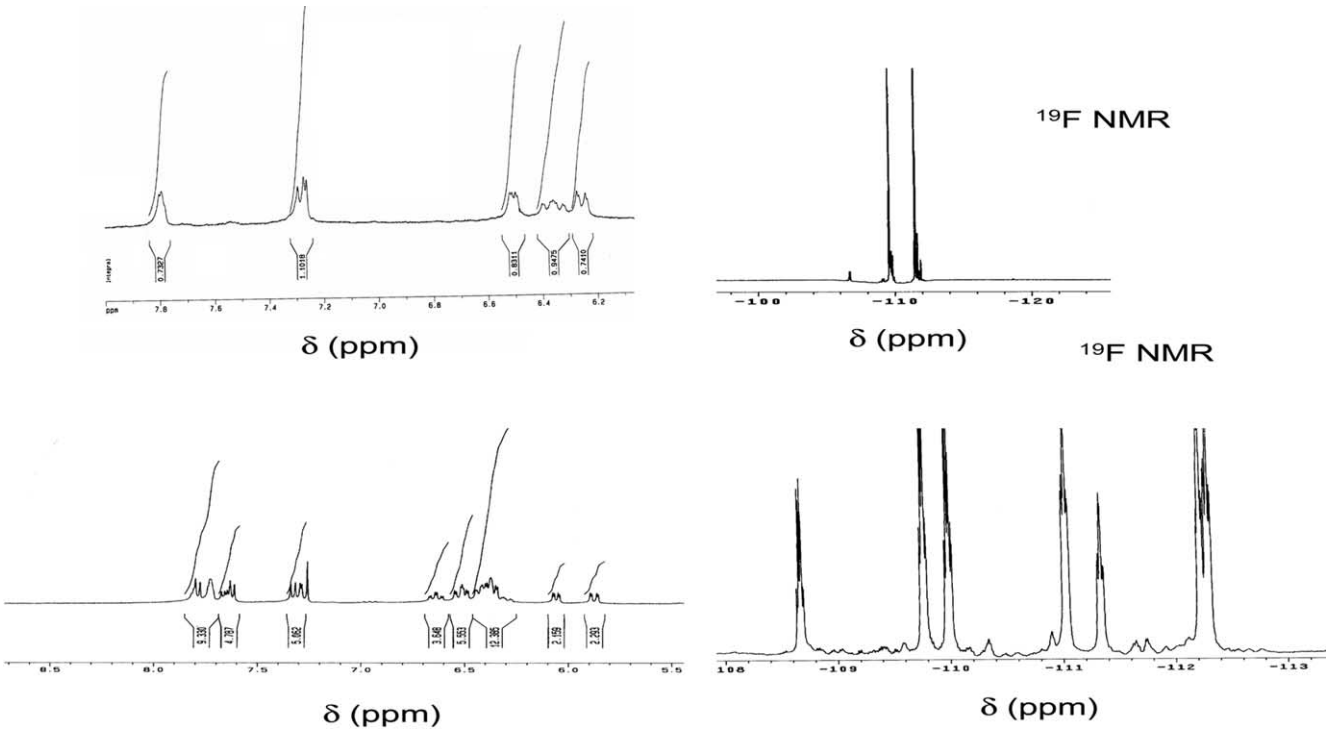

Fig. 1. ^{1}H and ^{19}F NMR spectra of *fac*-Ir(F_2MeOppy)$_3$ (top) and *mer*-Ir(F_2MeOppy)$_3$ (bottom), clearly distinguish the structures.

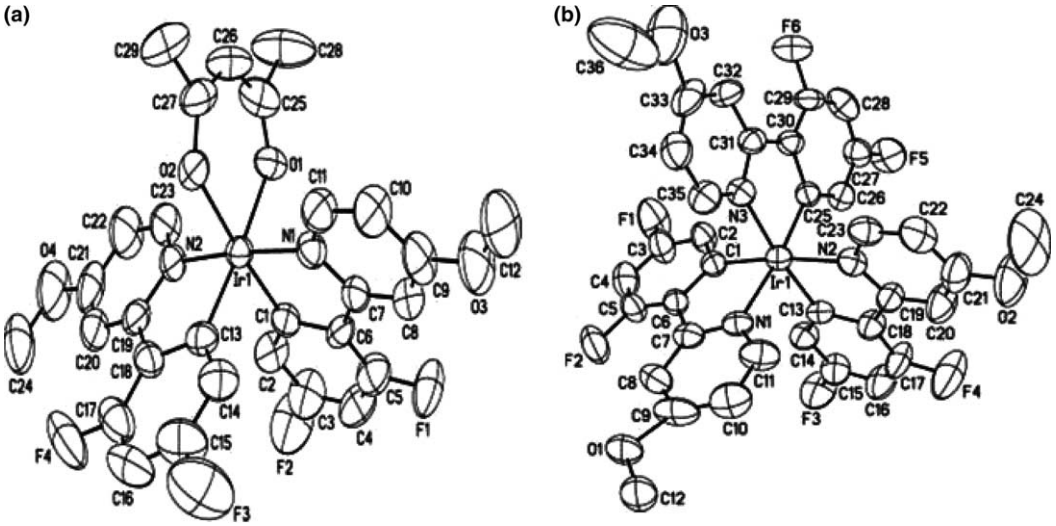

Fig. 2. The ORTEP drawings of (a) $Ir(F_2MeOppy)_2(acac)$ and (b) *fac*-$Ir(F_2MeOppy)_3$; the thermal ellipsoids for the image represent 50% probability.

Table 1
Crystal data and structure refinement for *fac*-$Ir(F_2MeOppy)_3$ and $Ir(F_2MeOppy)_2(acac)$

	fac-Ir($(F_2$ MeOppy$)_3$	Ir(F_2 MeOppy$)_2$ (acac)
Empirical formula	$C_{36}H_{28}F_6IrN_3O_5$	$C_{29}H_{23}F_4IrN_2O_4$
Formula weight	888.81	731.69
Temperature (K)	295(2)	296(2)
Wavelength (Å)	0.71073	0.71073
Crystal system	triclinic	monoclinic
Space group	$P\bar{1}$	$P2_1/c$
Unit cell dimensions		
a (Å)	12.2277(5)	8.1323(7)
b (Å)	12.3887(5)	18.9904(15)
c (Å)	24.4856(10)	17.2636 (14)
α (°)	93.103(1)	
β (°)	103.427(1)	90.777(2)
γ (°)	104.939(1)	
Volume (Å^3)	3460.1(2)	2665.9(4)
Z	4	4
D_{calc} (Mg/m^3)	1.706	1.823
Absorption coefficient (mm^{-1})	3.938	5.075
F(000)	1744	1424
Crystal size (mm)	$0.20 \times 0.20 \times 0.10$	$0.30 \times 0.20 \times 0.20$
θ Range for data collection	0.86–28.33	1.59–28.30
Index ranges	$-16 \leqslant h \leqslant 16$, $-16 \leqslant k \leqslant 16$, $-32 \leqslant l \leqslant 32$	$-10 \leqslant h \leqslant 9$, $-24 \leqslant k \leqslant 24$, $-20 \leqslant l \leqslant 23$
Reflections collected	41 099	17 219
Independent reflections [R_{int}]	17 088 [0.0514]	6331 [0.0432]
Completeness to θ (%)	99.0 (23.33)	95.5 (23.3)
Absorption correction	empirical	empirical
Maximum and minimum transmission	0.97346 and 0.59790	0.93848 and 0.71891
Refinement method	full-matrix least-squares on F^2	full-matrix least-squares on F^2
Data/restraints/parameters	17 088/1/941	6331/0/365
Goodness-of-fit on F^2	0.917	0.892
Final R indices [$I > 2\sigma(I)$]	$R_1 = 0.0443$, $wR_2 = 0.1034$	$R_1 = 0.0378$, $wR_2 = 0.0894$
R indices (all data)	$R_1 = 0.0971$, $wR_2 = 0.1178$	$R_1 = 0.0779$, $wR_2 = 0.958$
Largest differential peak and hole (e Å^{-3})	1.638 and −0.704	2.973 and −2.353

sitions of the ligands in both the complexes exhibit pseudo-octahedral geometry around the metal center. The C–C and C–N intraligand bond lengths and angles are within normal ranges expected for cyclometallated iridium(III) complexes and similar to the values reported for $(C^\wedge N)_2Ir(acac)$ [5e], *fac*-$Ir(C^\wedge N)_3$ [15,16] and

Table 2
Selected bond distances [Å] for *fac*-Ir($(F_2MeOppy)_3$ and Ir$(F_2MeOppy)_2$(acac)

fac-Ir($(F_2MeOppy)_3$		Ir$(F_2MeOppy)_2$(acac)	
Atom (1)–atom (2)	Distance (Å)	Atom (1)–atom (2)	Distance (Å)
Ir(1)–C(1)	2.017(7)	Ir(1)–C(13)	1.976(6)
Ir(1)–C(25)	2.020(6)	Ir(1)–C(1)	1.982(6)
Ir(1)–C(13)	2.021(7)	Ir(1)–N(1)	2.028(5)
Ir(1)–N(3)	2.113(6)	Ir(1)–N(2)	2.043(5)
Ir(1)–N(1)	2.117(6)	Ir(1)–O(1)	2.135(4)
Ir(1)–N(2)	2.131(6)	Ir(1)–O(2)	2.136(4)

$(C^N)_2Ir(\mu\text{-}Cl)Ir(C^N)_2$ [16] complexes. The *mer*-Ir$(F_2MeOppy)_3$ complex should have the same disposition of F_2MeOppy ligand as found in Ir$(F_2MeOppy)_2$(acac). The mutually *trans*-disposed Ir–N bonds in Ir$(F_2MeOppy)_2$(acac) have shorter bond lengths (Table 2) in comparison with those in *fac*-Ir$(F_2MeOppy)_3$ where the bond lies in a *trans* position (Fig. 2(b)) to the strong *trans* influencing phenyl group. Another point to be noted is that the weak *trans* influence of the acetylacetonate ligand leads to shorter Ir–C bonds for the Ir$(F_2MeOppy)_2$(acac) complex than those observed in *fac*-Ir$(F_2MeOppy)_3$, as indicated in Table 2.

3.3. Photophysical properties

The solution UV–Vis absorption and PL spectra of all these complexes have been measured. The UV–Vis absorption spectra of these complexes show intense bands appearing in the ultraviolet part of the spectrum between 240 and 340 nm. The measured energies and the extinction coefficients are comparable to those of the free ligand, which helped us to assign the bands as spin allowed $^1(\pi\text{–}\pi^*)$ transitions of the ligand. These ligand-centered bands are accompanied by weaker transitions with lower energy extending into the visible region from 350 to 400 nm (Fig. 3). With reference to the previous photophysical studies of cyclometallated complexes of the iridium(III) system [17], these absorption features are assigned to intra-ligand (IL) $\pi\text{–}\pi^*$ ($F_2MeOppy^-$) and also spin-allowed metal-to-ligand charge transfer ^{1}MLCT [$d\pi$ (Ir) $\rightarrow \pi$ $F_2MeOppy^-$)] transitions. In addition, spectra of all the complexes exhibit weaker absorption tails toward the further lower energy region (400–470 nm) (Fig. 3), which may be recognized as the spin-forbidden ^{3}MLCT [$d\pi$ (Ir) $\rightarrow \pi^*$ ($F_2MeOppy^-$)] transitions. The high intensity of these MLCT bands (shown by the extinction coefficients in the Table 3) has been attributed to an effective mixing of these charge transfer transitions with higher lying spin-allowed transitions on the cyclometallated ligand, which is facilitated by the strong spin–orbit coupling of the iridium(III) center. The energy of the MLCT transitions for the *fac*-isomer is comparatively higher than those of the rest of the complexes. These MLCT bands in the *fac*-isomer are more prominent and easily distinguishable as compared to its *mer*-counterpart, which is indicated in Fig. 3. The lowest energy transitions show blue-shifted absorption with increasing polarity of the solvents (i.e., toluene → chloroform → acetone → methanol). As shown in Fig. 4, the solution PL emission spectra of all the complexes exhibit structured features. These facts support that the lowest excited states of the complexes have a mixed ligand centered (LC) as well as MLCT character. As shown in Fig. 4, the PL intensity of the *fac*-isomer is much higher and exhibits ~6 nm hypsochromic shift with respect to its *mer*-counterpart. Similarly, the PL intensity of the Ir$(F_2MeOppy)_2$(acac) complex is found to be much higher and its emission spectrum much sharper relative to that of Ir$(F_2MeOppy)_2$(pic), whose spectrum is red-shifted, broad and

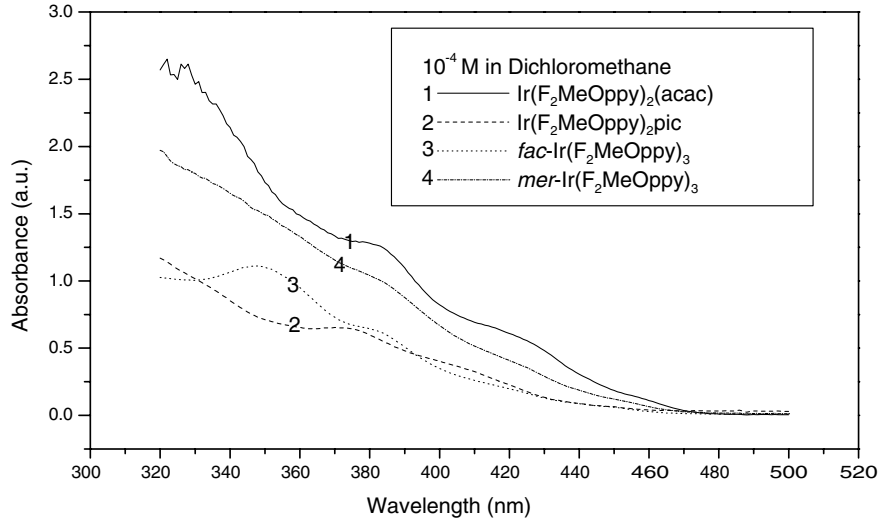

Fig. 3. UV–Vis absorption spectra for bis-and tris-cyclometallated complexes investigated in this work.

Table 3
Photophysical and electrochemical data for the bis and tris-(F_2MeOppy) cyclometallated iridium(III) complexes

Complex	Absorbance[a] λ (nm) (logε)	Emission λ_{max} (nm)		Relative quantum efficiency[a,c]	Redox $E^{ox}_{1/2}$ (V)[a]	HOMO (eV)	Lifetime (μs)
		Solution[a,b]	Film[b]				
Ir(F_2MeOppy)$_2$(acac)	383 (4.1); 419 (3.8)	471	469	0.60	0.508	5.3	0.59
Ir(F_2MeOppy)$_2$(pic)	375 (3.8); 411 (3.5)	509	485	0.82	0.661	5.5	0.84
fac-Ir(F_2MeOppy)$_3$	348 (4.1); 383 (3.8)	471	464	0.95	0.551	5.4	0.74
mer-Ir(F_2MeOppy)$_3$	384 (4.0); 420 (3.6)	477	468	0.41	0.345	5.6	0.68

[a] Solvent used dichloromethane.
[b] Excitations used 384, 374, 378 and 380 nm for solutions and 279, 270, 273 and 276 nm for thin films.
[c] Values are reported relative to Cp_2Fe/Cp_2Fe^+.

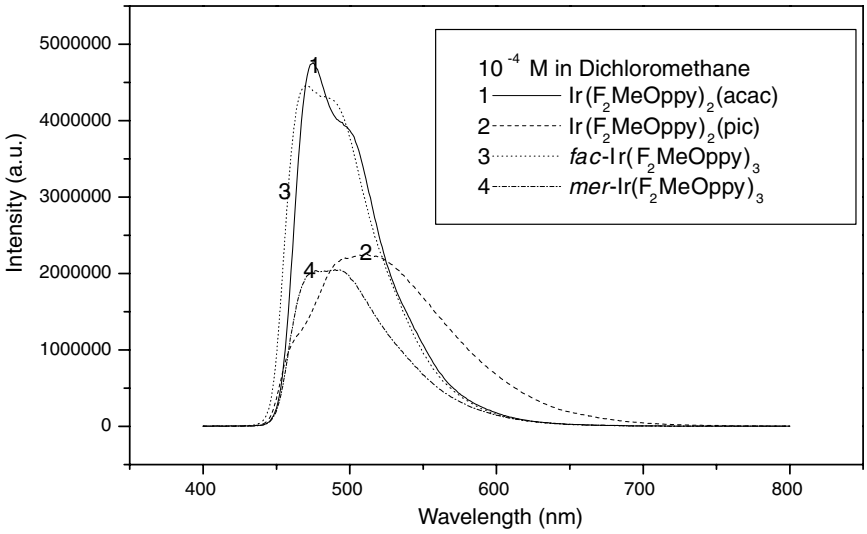

Fig. 4. Room temperature solution PL spectra for all the complexes in CH_2Cl_2.

featureless. The solution spectrum of Ir(F_2MeOppy)$_2$-(pic) also markedly differs from its thin-film emission spectrum (Fig. 5), which shows blue-shifted emission to a larger extent (~30 nm). It has also been observed that the nature of the emission spectra of Ir(F_2MeOppy)$_2$-(pic) is red-shifted in order of increasing polarity of the solvents, which suggest that the energy of the lowest emitting state of Ir(F_2MeOppy)$_2$(pic) is highly solvent dependent. The thin-film spectra for the other complexes, as shown in Fig. 5, exhibit blue-shifted emission to a smaller extent (~5–8 nm) as compared to their respective solution spectra.

The complexes, Ir(F_2ppy)$_2$(acac) and Ir(F_2ppy)$_2$(pic) [F_2ppy = 2-(2,4-difluorophenyl)pyridyine], have been reported [6d,7] and well characterized. The strong electron-donating methoxy substituent was incorporated onto the LUMO containing pyridyl ring of F_2ppy, and, therefore, it raised the LUMO energy and thereby increased the HOMO–LUMO energy gap. Hence, the complex Ir(F_2MeOppy)$_2$(acac) (λ_{max} = 471 nm) shows the expected blue-shifted emission as compared to the reported complex, Ir(F_2ppy)$_2$(acac) (λ_{max} = 476 nm). It is also known that Ir(F_2ppy)$_2$(pic) (λ_{max} = 456 nm) exhibits blue shifted emission compared to its acetylacetonate analogue, Ir(F_2ppy)$_2$(acac) (λ_{max} = 476 nm). But in our case, Ir(F_2MeOppy)$_2$(pic) (λ_{max} = 509 nm) shows a wide red shifted emission compared to its acetylacetonate analogue (λ_{max} = 471 nm). We have measured the solution quantum efficiency of the complexes and the results are shown in Table 3. The *fac*-isomer shows a much higher quantum efficiency as compared to its counter *mer*-isomer. Furthermore, as shown in Table 3, the measured lifetime for thin film samples falls into the microsecond regime, which evidence the lowest excited states are the triplet-emitting states for these complexes. The short life-time also indicates that there is strong spin–orbit coupling in the presence of heavy metal iridium(III).

3.4. Electrochemistry

The electrochemical properties of the bis- and tris-cyclometallated complexes were examined by cyclic voltammetry. Redox potentials, given in Table 3, were measured relative to an internal ferrocene reference (Cp_2Fe/Cp_2Fe^+ = 0.62 versus SCE in dichloromethane solvent). All of these complexes showed reversible oxidation, in

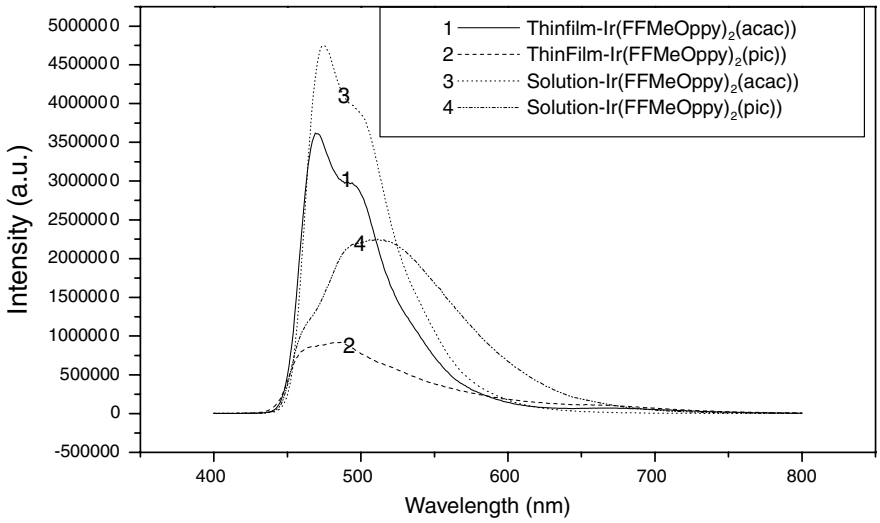

Fig. 5. Comparison of thin-film and solution PL spectra for $Ir(F_2MeOppy)_2X$ (X = acac and pic).

the range from 0.34 to 0.67 V. The *fac*-isomer has oxidation potentials ca. ~200 mV more positive than the corresponding *mer*-form (i.e., fac_{ox}: 0.55 V; mer_{ox}: 0.34 V), whereas the reduction potential for the *fac*-form is slightly more negative than that of the *mer*-isomer (i.e., fac_{red}: −2.67 V; mer_{red}: −2.62 V). It was known that for phenyl-pyridyl based complexes, the oxidation processes involve the Ir–phenyl center (major HOMO contribution), while reduction processes occur primarily on the heterocyclic portion (major LUMO contribution) of the ligand [6]. The difference in electrochemical properties between *facial* and *meridional* isomers can be rationalized by the presence of mutually *trans* phenyl rings of the ligands in the *mer*-isomer, whereas in the *facial* form all the phenyls are *cis* (Fig. 2(b)) with respect to one another. Electron-rich sigma phenyl ligands normally exhibit a very strong *trans* influence and *trans* effect, which results in a lengthening of the *transoid* Ir–C bonds and hence destabilization of the HOMO to a significant extent, which is supported by the HOMO–LUMO energy calculations using redox data and absorption wavelength, summarized in Table 3. Therefore, it is concluded that the *mer*-isomer is easier to oxidize than the *fac*-isomer.

3.5. Description and performance of OLED devices

Initially, we fabricated an electroluminescent device D-1 with structure ITO/CF_x/NPB (300 Å)/CBP + 7% dopant (200 Å)/BAlq (300 Å)/Alq_3 (150 Å)/LiF (10 Å)/Al (2000 Å) (the molecular structures of each compound used in the EL device are shown in Scheme 3) using the complex $Ir(F_2MeOppy)_2(acac)$ as a dopant in the emitting layer. Fig. 6 shows the EL emission spectra of the device where a broad and long tail extending up to 735 nm was observed. Clearly, the emission appearing in the green and red regions is attributed to the leakage of holes into the BAlq and Alq_3 layers and the consequent recombination in those layers infers that BAlq is not an effective hole blocker (HB) for deep-blue electroluminescent material (Scheme 4a). Consequently, we replaced BAlq with BCP, which has a comparatively higher HOMO level (6.5 eV) as compared to BAlq (6.0 eV). Accordingly, we fabricated another device by incorporating the same dopant, $Ir(F_2MeOppy)_2(acac)$ (D-2) into the emitting layer, with BAlq replaced by BCP as a hole blocker. No observation of a broad emission was found in this device, but another extra emission was observed at ca. 425 nm, which was attributed to the NPB hole transport material as shown in Fig. 6. The external luminance efficiency and the power efficiency is found to be 0.66 cd A^{-1} and 0.22 lm W^{-1}, respectively, at a current density of 20 mA cm^{-2}, as indicated in Fig. 7. The lowest triplet energy levels for the dopant, $Ir(F_2MeOppy)_2(acac)$ and the host, CBP are 2.64 [1] and 2.56 eV [12], respectively, which suggests that the endothermic energy transfer [7] is being operated between the host and the dopant. This type of energy transfer in an EL device is not completely favorable for blue-emitting dopants (Scheme 4b) [c]. The fabrication of another EL device was carried out with the host *m*CP, having a wider band gap, i.e., 2.90 eV [18]. The layer sequences and the thicknesses of each layer were kept constant as before. The comparisons of device performance of D-2 and D-3 have been shown in Table 4. As indicated in Fig. 7, in this case the external quantum efficiency and the power efficiency are improved and found to be 1.63 cd A^{-1} and 0.47 lm W^{-1} at 20 mA cm^{-2} current density, respectively, as compared

[1] The triplet emitting state of $Ir(F_2MeOppy)_2(acac)$ has been calculated from the maximum emission wavelength at 298 K.

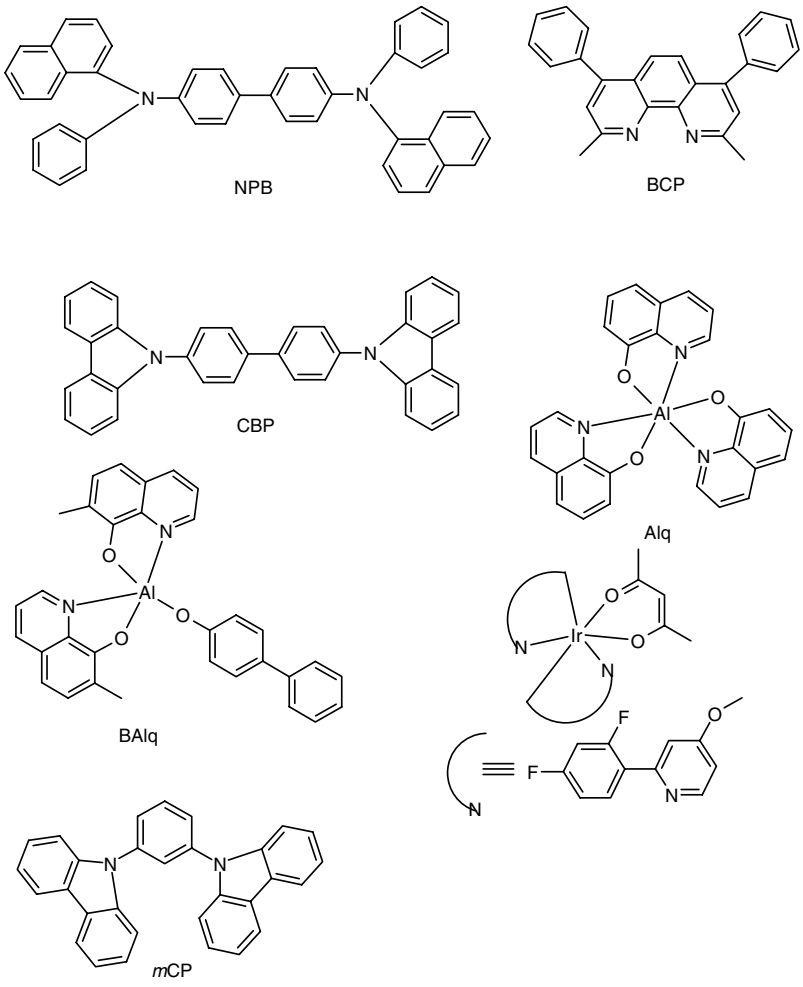

Scheme 3.

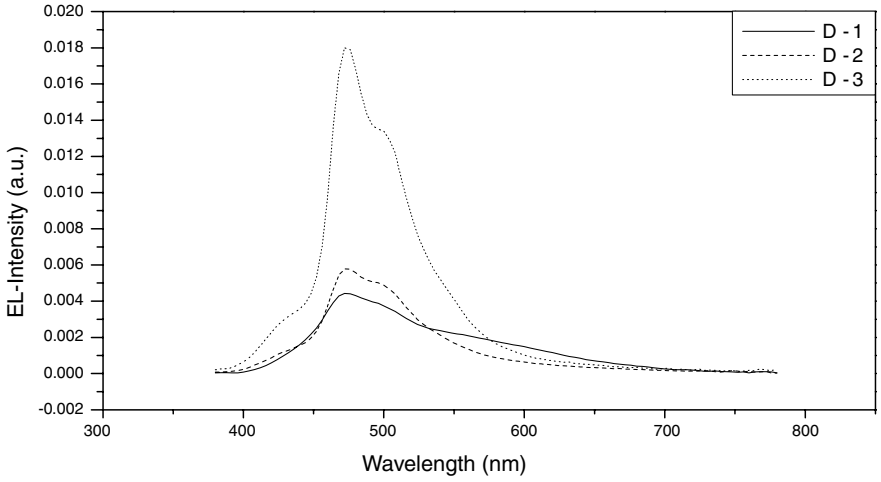

Fig. 6. Comparative electroluminescent emission spectra of devices D-1, D-2 and D-3.

to the previous devices. This device shows a luminance value of 326 cd m^{-2} at 20 mA cm^{-2} current density, that is also higher than that of the former device (133 cd m^{-2} at 20 mA cm^{-2}) (Figs. 8(a) and (b)). Hence the exothermic triplet energy transfer to the blue dopant Ir(F_2-MeOppy)$_2$(acac) is more efficient when using the wider band gap host *m* CP. The comparisons of *I–V* curves have also been shown in Fig. 8(a) and (b).

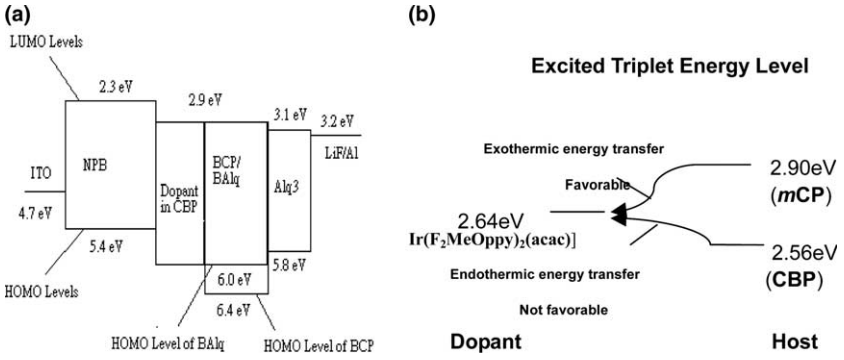

Scheme 4.

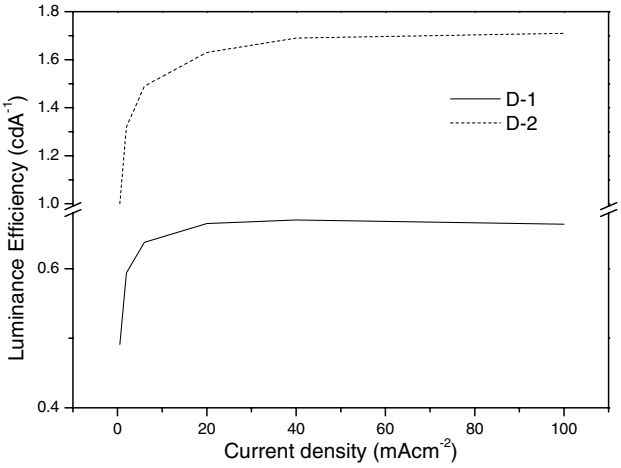

Fig. 7. Comparative plot of luminescent efficiency vs. current density of D-2 and D-3 devices.

Table 4
Comparisons of the EL performances of the devices with structure: ITO/CHF_3/NPB (300 Å)/Host + 7% dopant (200 Å)/BAlq (300 Å)/Alq_3(150 Å)/LiF (10 Å)/Al (2000 Å), Host − CBP for D-2; *m*CP for D-3

	D-2	D-3
EL color	blue	blue
Peak wavelength (nm)	472	472
CIE-x at 20 mA cm^{-2}	0.19	0.17
CIE-y	0.31	0.30
Luminance (cd m^{-2} at 20 mA cm^{-2})	133	327
External quantum efficiency (cd A^{-1} at 20 mA cm^{-2})	0.66	1.63
Power efficiency (lm W^{-1} at 20 mA cm^{-2})	0.22	0.88

All these parameters have been recorded at 20 mA cm^{-2}.

4. Conclusion

We have synthesized four iridium(III)-based phosphorescent dopants that emit in the blue range, using the same cyclometallated ligand, 2-(2′,4′-difluorophenyl)-4-methoxypyridine. These complexes show different maximum emission wavelengths and quantum efficiencies with respect to the ancillary ligands (actylacetonate and picolinate) and the types of isomerism. The strong

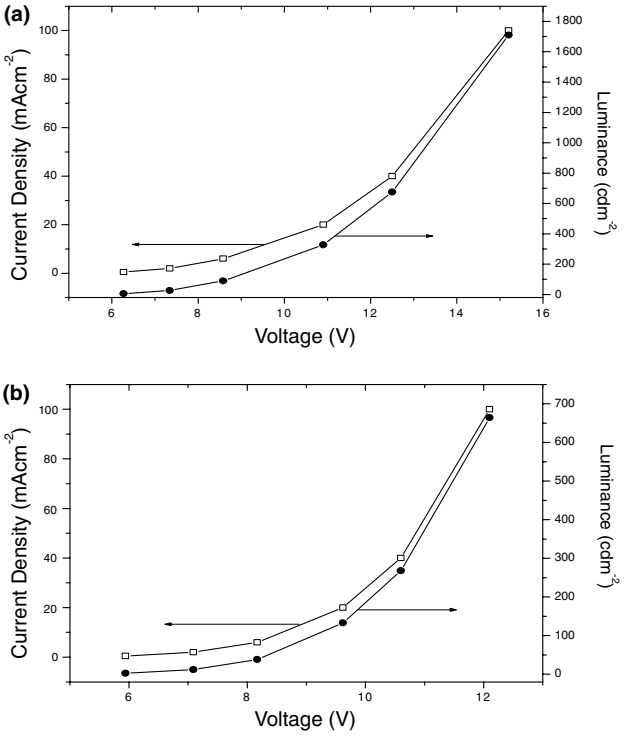

Fig. 8. Comparative plot of current density, voltage and luminance characteristics for the devices 2 (presented in **b**) and 3 (presented in **a**).

trans-influence in the *meridional* isomer leads to less stable, broader, red-shifted and lower quantum efficiencies than the *facial* counterpart. Three EL devices were fabricated. It can be stated that BAlq is not a good hole blocker in the EL device for a blue-emitting phosphorescent dopant. It has also been shown that the wider band gap host *m*CP shows good EL performances with respect to the host CBP having a relatively lower band gap, for the same blue-emitting iridium(III) dopant.

5. Supplementary data

Crystallographic data for the structural analysis have been deposited with the Cambridge Crystallographic

Data Centre, CCDC Nos. 228968 and 228969 for compounds $Ir(F_2MeOppy)_2(acac)$ and *fac*-$Ir(F_2MeOppy)_3$, respectively. Copies of this information may be obtained free of charge from the Director, CCDC, 12 Union Road, Cambridge, CB2 1EZ, UK (fax: +44 1223 336033; email: deposit@ccdc.cam.ac.uk or www:http://www.ccdc.cam.ac.uk).

Acknowledgement

This research is supported by the Program for Promoting University Academic Excellence from the Ministry of Education, Taiwan, Republic of China under the Contract PPAEU91-E-FA04-2-4-(B).

References

[1] (a) J.K. Lee, D. Yoo, M.F. Rubner, Chem. Mater. 9 (1997) 1710;
(b) F.G. Gao, A. Bard, J. Am. Chem. Soc. 122 (2000) 7426.
[2] (a) Y. Li, Y. Liu, J. Guo, F. Wu, W. Tian, B. Li, Y. Wang, Synth. Met. 118 (2001) 175;
(b) K. Wang, L. Huang, L. Gao, L. Jin, C. Huang, Inorg. Chem. 41 (2002) 3353.
[3] F.G. Gao, A.J. Bard, Chem. Mater. 14 (2002) 3465.
[4] (a) C.-L. Lee, K.B. Lee, J.-J. Kim, Appl. Phys. Lett. 77 (2000) 2280;
(b) R.R. Das, C.-L. Lee, J.-J. Kim, Mat. Res. Soc. Symp. Proc. 708 (2002) BB3.39.1;
(c) J.P.J. Markham, S.-C. Lo, S.W. Magennis, P.L. Burn, I.D.W. Samuel, Appl. Phys. Lett. 80 (2002) 2645.
[5] (a) I.R. Laskar, T.-M. Chen, Chem. Mater. 16 (2004) 111;
(b) T. Tsuzuki, N. Shirasawa, T. Suzuki, S. Tokito, Adv. Mater. 15 (2003) 1455;
(c) A. Beeby, S. Bettington, I.D.W. Samuel, Z.J. Wang, Mater. Chem. 13 (2003) 80;
(d) M.K. Nazeeruddin, R. Humphry-Baker, D. Berner, S. Rivier, L. Zuppiroli, M. Graetzel, J. Am. Chem. Soc. 125 (2003) 8790;
(e) S. Lamansky, P. Djurovich, D. Murphy, F. Abdel-Razzaq, R. Kwong, I. Tsyba, M. Bortz, B. Mui, R. Bau, M.E. Thompson, Inorg. Chem. 40 (2001) 1704;
(f) S. Lamansky, P. Djurovich, D. Murphy, F. Abdel-Razzaq, H.-F. Lee, C. Adachi, P.E. Burrows, S.R. Forrest, M.E. Thompson, J. Am. Chem. Soc. 123 (2001) 4304;
(g) M.E. Thompson, S. Lamansky, P. Djurovich, D. Murphy, F. Abdel-Razzaq, R. Kwong, S.R. Forrest, M.A. Baldo, P.E. Burrows, patent US 20020034656A1;
(h) M.A. Baldo, M.E. Thompson, S.R. Forrest, Pure Appl. Chem. 71 (1999) 2095.
[6] (a) A.B. Tamayo, B.D. Alleyne, P.I. Djurovich, S. Lamansky, I. Tsyba, N.N. Ho, R. Bau, M.E. Thompson, J. Am. Chem. Soc. 125 (2003) 7377;
(b) R.J. Holmes, W. D'Andrade, S.R. Forrest, X. Ren, J. Li, M.E. Thompson, Appl. Phys. Lett. 83 (2003) 3818;
(c) S. Tokito, T. Iijima, Y. Suzuri, H. Kita, T. Tsuzuki, F. Sato, Appl. Phys. Lett. 83 (2003) 569;
(d) S. Lamansky, M.E. Thompson, V. Adamovich, P.I. Djurovich, C. Adachi, M.A. Baldo, S.R. Forrest, Kwong, patent US 20020182441A1.
[7] C. Adachi, R.C. Kwong, P. Djurovich, V. Adamovich, M.A. Baldo, M.E. Thompson, S.R. Forrest, Appl. Phys. Lett. 79 (2001) 2082.
[8] P. Coppo, E.A. Plummer, L.D. Cola, Chem. Commun. 15 (2004) 1774.
[9] G.C. Finger, L.D. Starr, J. Am. Chem. Soc. 81 (1959) 2674.
[10] S.J. Connon, A.F. Hegarty, Tetrahedron Lett. 42 (2001) 735.
[11] G.M. Sheldrick, SAINT; Bruker Analytical X-ray Instrument Division, Madison, WI, 1998.
[12] G.M. Sheldrick, SHELXTL Programs, version 5.1; Bruker AXS GmbH, Karlsruhe, Germany, 1998.
[13] J. Demas, G.A. Crosby, J. Phys. Chem. 75 (1971) 991.
[14] K.A. King, P.J. Spellane, R.J. Watts, J. Am. Chem. Soc. 107 (1985) 1431.
[15] V.V. Grushin, N. Herron, D.D. LeCloux, W.J. Marshall, V.A. Petrov, Y. Wang, New Chem. Commun. (2001) 1494.
[16] F.O. Graces, K. Dedian, N.L. Keder, R.J. Watts, Acta Crystallogr. C49 (1993) 1117.
[17] (a) F.O. Graces, K.A. King, R.J. Watts, Inorg. Chem. 27 (1988) 3464;
(b) S. Serroni, A. Juris, S. Campagna, M. Venturi, G. Denti, V. Balgani, J. Am. Chem. Soc. 116 (1994) 9086;
(c) P.M. Griffiths, F. Loiseou, F. Puntoriero, S. Serroni, S. Campagna, Chem. Commun. (2000) 2297.
[18] R.J. Holmes, S.R. Forrest, Y.-J. Tung, R.C. Kwong, J.J. Brown, S. Garon, M.E. Thompson, Appl. Phys. Lett. 82 (2003) 2422.